Nonlocal interactions and supersolidity of moiré excitons

Aleksi Julku ◉

Center for Complex Quantum Systems, Department of Physics and Astronomy, Aarhus University,
Ny Munkegade 120, DK-8000 Aarhus C, Denmark

Heterobilayer transition metal dichalcogenide (TMDC) moiré systems provide an ideal framework to investigate strongly correlated physics. Here we theoretically study bosonic many-body phases of excitons in moiré TMDCs. By using two moiré models and cluster mean-field theory, we reveal that, due to nonlocal Coulomb interactions, moiré excitons can feature exotic supersolid phases, i.e., superfluids of broken translational invariance, and correlated insulating states. The correlated phases exist at experimentally accessible temperatures and are tunable via the twist angle and exciton density.

Introduction. Rapid advances in nanofabrication techniques have allowed for experimental realizations of multilayer van der Waals moiré heterostructures, where lattice mismatch or a twist angle between monolayers, results in a tunable long-wavelength potential for electrons [1–3]. Moiré potential leads to localized electrons, reducing their kinetic energy and thus enhancing the role of interactions. Moiré systems, therefore, serve as versatile platforms to study strongly correlated electronic systems. Prominent interaction-driven phases observed in moiré systems include superconductivity in twisted bilayer and multilayer graphene [4–6] and correlated electronic states, such as Wigner crystals, stripes, and Mott insulators in bilayer transition metal dichalcogenides (TMDC) [7–15].

Moiré TMDCs are also an ideal platform for revealing many-body effects of bosons. Namely, in TMDC monolayers, excitons, i.e. bound electron-hole pairs, can be optically created. Correspondingly, the moiré potential of electrons leads to formation of moiré excitons [9,16–25]. While most of the research has focused on probing moiré electrons with excitons [9,11,12,14,15,26], less attention has been given to possible bosonic many-body phases of moiré excitons. As the moiré potential allows the confinement of bosons to triangular or honeycomb lattice geometries [19], and as repulsive Coulomb interactions between moiré excitons can be very strong compared to their kinetic energy, it is tempting to expect that moiré excitons form Mott insulating phases. This was indeed predicted in a recent theoretical study [27] for a large range of tunable parameters. Moreover, the possibility to reach superfluidity of moiré excitons has also been speculated [27,28].

Due to the strong on-site interaction, weaker nonlocal interactions between excitons are often ignored. However, at sufficiently low densities the on-site interaction can, by virtue of hard-core boson constraint, be discarded so the nonlocal interactions become the dominant interaction channel. In this work, we theoretically study possible many-body phases of moiré excitons by taking into account nonlocal interactions. We employ two different continuum models [18,29], from

which we derive the effective tight-binding models for moiré excitons and compute nonlocal exciton-exciton interactions. By using cluster mean-field (CMF) theory [30–34], we show that in addition to possible conventional Mott and superfluid states, moiré excitons can also exhibit more exotic many-body states, namely correlated insulating and superfluid phases of broken translational invariance. The latter is widely known as the *supersolid* phase. We show that these states are accessible using reasonable twist angles and exciton densities, and experimentally accessible temperatures.

Hamiltonian. We consider moiré excitons of a TMDC heterobilayer system of layers 1 and 2. TMDC monolayers have a hexagonal lattice structure and direct band gaps at the corners of their hexagonal Brillouin zone (BZ), namely in the K and K' valleys [35–37]. Small lattice constant mismatch or twist angle θ between layers causes the interlayer electron tunneling to hybridize the low-energy states of two layers in the K and K' valleys [18,38]. This gives a rise to moiré flat bands of excitons, long moiré periodicity a_m, and reduced moiré BZ (mBZ), see Figs. 1(a)–1(c). As excitons can be created valley-selectively [35,39–44], we from now on consider only the K-valley excitons and small twist angles $\theta \sim 0 - 4°$.

We study the many-body properties of moiré excitons by employing two different one-particle continuum Hamiltonians. The first one, which we call hybridized moiré exciton model and denote H_H, has been used successfully in Refs. [17,18] to study the hybridization of intralayer and interlayer excitons in moiré structures. The model treats the interlayer electron tunneling $t(\mathbf{k}, \mathbf{k}')$ from momentum $\mathbf{k}'$ to $\mathbf{k}$ in the microscopic level as $t(\mathbf{k}, \mathbf{k}') \propto \delta_{\mathbf{k},\mathbf{k}'} + \delta_{\mathbf{k}-\mathbf{k}',\mathbf{b}_1^m} + \delta_{\mathbf{k}-\mathbf{k}',\mathbf{b}_2^m}$ [$\mathbf{b}_i^m$ are the moiré reciprocal vectors, see Fig. 1(b)], which leads to the emergence of moiré excitons (see Supplemental Material (SM) [45] for further details).

The second model, which we denote H_E, treats the moiré effects with a slowly varying effective potential $\Delta(\mathbf{r})$ ($\mathbf{r}$ being the spatial coordinate) i.e., the single-particle Hamiltonian for excitons is simply $H_E = -\nabla^2/2m + \Delta(\mathbf{r})$, where m is the exciton mass. We call this as an effective potential model,
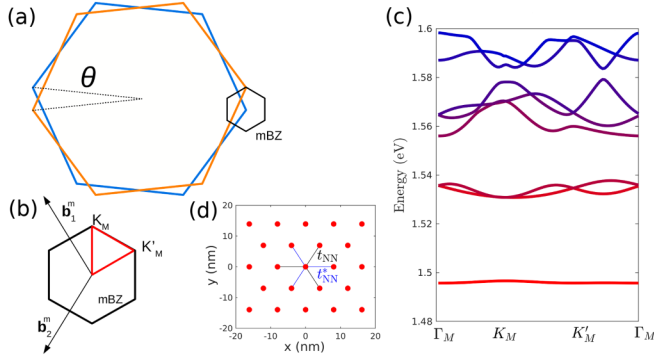
FIG. 1. (a) Schematic of the moiré system in the momentum space. Blue (orange) hexagon depicts the BZ of layer 1 (2) and black hexagon presents the moiré BZ (mBZ) in the K valley. (b) K-valley mBZ. The momentum space is spanned by vectors $\mathbf{b}_1^m$ and $\mathbf{b}_2^m$. The red path gives the x axis of panel (c). (c) Moiré exciton K-valley spin-down band structure at $\theta = 0.5°$ obtained for MoSe/WS$_2$ with H_H. (d) Corresponding triangular tight-binding model for the lowest band moiré excitons, characterized by the NN hopping t_{NN} and moiré periodicity a_m.

and it has been widely used to study moiré electrons [46–49] and excitons [16,19,27,29,50]. Recent first-principles studies [51] have argued that continuum models are sufficient to capture the nature of the lowest energy moiré excitons, the primary focus of this work. Following the experimental works of [16,17], we apply H_H (H_E) to study a hybrid moiré excitons (moiré interlayer excitons) in a MoSe$_2$/WS$_2$ (MoSe$_2$/WSe$_2$) heterobilayer system.

Both H_H and H_H yield one-particle Hamiltonians in the form $H_0 = \sum_{n\mathbf{k}\in\text{mBZ}} \epsilon_{\mathbf{k}n}\gamma_{\mathbf{k}n}^\dagger\gamma_{\mathbf{k}n}$, where n is the band index and $\gamma_{\mathbf{k}n}$ annihilates a moiré exciton at momentum $\mathbf{k}$ and energy $\epsilon_{\mathbf{k}n}$ [45]. For both the models, the lowest energy band $\epsilon_{\mathbf{k}1}$ at small θ is extremely flat and well isolated from higher bands by a large band gap (see Fig. 1(c) and SM [45]). Subsequently, the Wannier functions of the lowest moiré exciton band form a triangular lattice characterized by the nearest-neighbor hopping t_{NN} [45], see Fig. 1(d). We thus write the effective tight-binding Hamiltonian of the excitons in the lowest moiré band as

$$H = \sum_{<i,j>} t_{ij}x_i^\dagger x_j + \sum_i U_0 x_i^\dagger x_i^\dagger x_i x_i + \sum_{i,j} U_{ij} x_i^\dagger x_j^\dagger x_j x_i, \quad (1)$$

where x_i annihilates a moiré exciton in lattice site i, t_{ij} describes hopping from site i to j, U_0 is the repulsive on-site interaction, U_{ij} denotes the nonlocal interactions between sites i and j, and the sum over the hopping terms is limited to nearest-neighboring sites. Interaction terms arise due to Coulomb interactions between excitons, and the values of t_{ij}, U_0, and U_{ij} depend on the chosen continuum model. The hopping values are obtained as the Fourier transform of the energies of the lowest moiré band, i.e., $t_{ij} = \frac{1}{N}\sum_{\mathbf{k}\in\text{mBZ}} \epsilon_{\mathbf{k}1} e^{-i\mathbf{k}\cdot(\mathbf{R}_i-\mathbf{R}_j)}$. Here, N is the number of moiré unit cells, and $\mathbf{R}_i$ denote the locations of moiré lattice sites.

Deriving interaction terms U_0 and U_{ij} is more involved and depends on the chosen model. We detail how to do this for H_H in the next section. In Fig. 2 we present U_0, nearest-neighbor
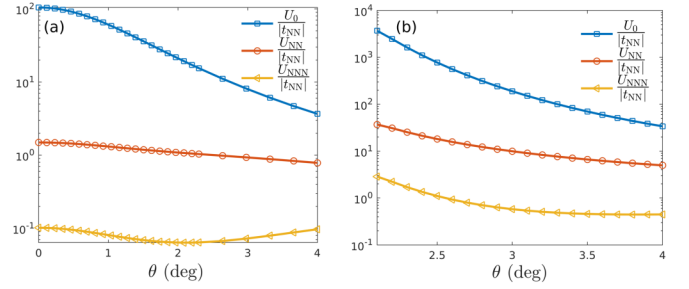

FIG. 2. (a) and (b) U_0, U_{NN}, and U_{NNN} with respect to $|t_{NN}|$ as a function of θ obtained with H_H and H_E continuum models, respectively.

(NN) and next-nearest-neighbor (NNN) interactions, U_{NN} and U_{NNN}, with respect to $|t_{NN}|$ as a function of θ for the two continuum models. In both cases, U_0 is the dominant energy scale, being roughly one to two orders of magnitude larger than U_{NN}. Furthermore, U_{NN} is comparable to t_{NN} in case of H_H and much larger than t_{NN} when using H_E. We also see that in the case of H_E, NNN interaction is comparable to t_{NN} and cannot be ignored. We thus keep the interactions up to the NN (NNN) terms when using H_H (H_E). In the case of moiré electrons, nonlocal interactions have been predicted to lead a rich landscape of many-body phases [47–49,52–54].

Exciton-exciton interactions. We now derive the interaction terms of Eq. (1) in the case of H_H (derivation for H_E is given in SM [45]). In this model, the moiré excitons consist of superpositions of intra and interlayer excitons labeled as $|X\rangle$, $|X'\rangle$, $|IX\rangle$, and $|IX'\rangle$. Intralayer excitons $|X\rangle$ ($|X'\rangle$) and holes of interlayer excitons $|IX\rangle$ ($|IX'\rangle$) reside in layer 1 (2). However, due to the permanent dipole moment of interlayer excitons, IX-IX, IX'-IX', and IX-IX' interactions are much larger than other interaction terms. Hence, we write the interaction Hamiltonian for the direct Coulomb interactions as

$$H_{\text{int}} = \frac{1}{2A}\sum_{\substack{\mathbf{k}\mathbf{k}'\mathbf{q}\\t\tilde{t}}} g_{t\tilde{t}}^{dir}(\mathbf{q})x_{t,\mathbf{k}+\mathbf{q}}^\dagger x_{\tilde{t},\mathbf{k}'-\mathbf{q}}^\dagger x_{\tilde{t},\mathbf{k}'}x_{t,\mathbf{k}}, \quad (2)$$

where A is the system area, $t,\tilde{t} \in \{IX,IX'\}$, $x_{t,\mathbf{k}}$ annihilates an interlayer exciton of momentum $\mathbf{k}$ and type t, $g_{tt}^{dir}(\mathbf{q})$ is the interaction vertex and the momenta sums are *not* limited to mBZ. We transfer to the moiré exciton basis:

$$H_{\text{int}} = \sum_{\substack{\mathbf{k}\mathbf{k}'\mathbf{q}\in\text{mBZ}\\ijkl}} \frac{g_{ijkl}^{dir}(\mathbf{k},\mathbf{k}',\mathbf{q})}{2A}\gamma_{\mathbf{k}+\mathbf{q}i}^\dagger\gamma_{\mathbf{k}'-\mathbf{q}j}^\dagger\gamma_{\mathbf{k}'k}\gamma_{\mathbf{k}l} \quad (3)$$

with

$$g_{ijkl}^{dir}(\mathbf{k},\mathbf{k}',\mathbf{q}) = \sum_{t,\tilde{t}}\sum_{\alpha\beta\gamma} g_{t\tilde{t}}^{dir}(\mathbf{q}+\mathbf{G}_\gamma)\langle u_{i,\mathbf{k}+\mathbf{q}}|t,\alpha+\gamma\rangle$$
$$\times \langle u_{j,\mathbf{k}'-\mathbf{q}}|\tilde{t},\beta-\gamma\rangle\langle\tilde{t},\beta|u_{k,\mathbf{k}'}\rangle\langle t,\alpha|u_{l,\mathbf{k}}\rangle. \quad (4)$$

Here $|u_{i,\mathbf{k}}\rangle$ is the periodic part of the moiré Bloch function for the ith band of momentum $\mathbf{k}$, and matrix elements $\langle t,\alpha|u_{i,\mathbf{k}}\rangle$ represent its components related to the exciton of type t at momentum $\mathbf{k}+\mathbf{G}_\alpha$ with $\mathbf{G}_\alpha \equiv q_\alpha\mathbf{b}_1^m + p_\alpha\mathbf{b}_2^m$ (q_α and p_α are integers).

The Coulomb interaction vertex $g_{t\tilde{t}}^{dir}(\mathbf{q})$ can be straightforwardly computed by deploying the excitonic wave functions $\phi(\mathbf{k})$ [45]. For example, the interaction vertex between two IX excitons is

$$g_{\mathrm{IX,IX}}^{dir}(\mathbf{q}) \approx \frac{e^2}{2q} \left\{ \frac{f(x_h^{\mathrm{IX}}\mathbf{q})^2}{\epsilon_{\mathrm{intra},2}(q)} + \frac{f(x_e^{\mathrm{IX}}\mathbf{q})^2}{\epsilon_{\mathrm{intra},1}(q)} \right.$$
$$\left. - \frac{2f(x_e^{\mathrm{IX}}\mathbf{q})f(x_h^{\mathrm{IX}}\mathbf{q})}{\epsilon_{\mathrm{inter}}(q)} \right\}. \quad (5)$$

Here e is the elementary charge, $f(\mathbf{k}) = \sum_{\tilde{\mathbf{q}}} \phi_{IX}^*(\tilde{\mathbf{q}})\phi_{IX}(\tilde{\mathbf{q}} + \mathbf{k})$ and x_e^{IX} (x_h^{IX}) is the relative electron (hole) mass of the IX exciton such that $x_e^{\mathrm{IX}} + x_h^{\mathrm{IX}} = 1$ [45]. The terms inside the wave brackets arise due to electron-electron, hole-hole and electron-hole Coulomb interactions, respectively. We have approximated the excitons to be tightly localized in the momentum space around the K-point [45]. Furthermore, we take into account the two-layer geometry via the momentum-dependent intralayer and interlayer dielectric functions, $\epsilon_{\mathrm{intra}}(q)$ and $\epsilon_{\mathrm{inter},l}(q)$ [55], derived in SM [45].

We rewrite Eq. (3) for the tight-binding model (1) by discarding all but the lowest moiré band and using the Wannier function expansion, i.e., $\gamma_{\mathbf{k}1} = \frac{1}{\sqrt{N}} \sum_i e^{i\mathbf{k}\cdot\mathbf{R}_i} x_i$ [45], to obtain

$$H_{\mathrm{int}} \approx \frac{1}{2A} \sum_{\mathbf{k}\mathbf{k}'\mathbf{q}\in\mathrm{mBZ}} g_{1111}^{dir}(\mathbf{k},\mathbf{k}',\mathbf{q})\gamma_{\mathbf{k}+\mathbf{q}1}^\dagger \gamma_{\mathbf{k}'-\mathbf{q}1}^\dagger \gamma_{\mathbf{k}'1}\gamma_{\mathbf{k}1}$$
$$= \sum_{a,b,c,d} g_{abcd} x_a^\dagger x_b^\dagger x_c x_d \quad (6)$$

with

$$g_{abcd} = \sum_{\mathbf{k}\mathbf{k}'\mathbf{q}} \frac{g_{1111}^{dir}(\mathbf{k},\mathbf{k}',\mathbf{q})}{2AN^2} \frac{e^{i\mathbf{k}'\cdot\mathbf{R}_c + i\mathbf{k}\cdot\mathbf{R}_d}}{e^{i(\mathbf{k}+\mathbf{q})\cdot\mathbf{R}_a + i(\mathbf{k}'-\mathbf{q})\cdot\mathbf{R}_b}}. \quad (7)$$

Equation (7) gives rise to different scattering processes such as direct and exchange interactions (g_{abba}, g_{abab}), interaction-assisted hopping g_{aaab}, and pair hopping g_{aabb}. The importance of such terms was highlighted in Ref. [49] for the case of moiré electrons. Here, however, the direct interaction is the dominant one and we discard nondirect terms to obtain Eq. (1).

Supersolidity of moiré excitons. As U_0 in (1) is much larger than other energy scales, it is presumable that the ground state is a Mott insulator when the exciton density n, i.e., the number of excitons per lattice site, is $n = 1$. However, for *smaller densities*, the ground state can be very different. Namely, U_0 is so large that for $n < 1$, one can employ the hard-core constraint (HCC), i.e., to limit the occupation number of each lattice site to be less than 2. HCC is accurate when $n < 1/A_{\mathrm{uc}}$, where A_{uc} is the area of the moiré unit cell. For example, with twist angle $\theta = 2°$, $1/A_{uc}^m = 3.1 \times 10^{-12}$ cm^{-2} for a MoSe$_2$/WS$_2$ structure. This density is to be contrasted with experimentally measured critical density n_c above which interlayer moiré excitons dissociate to free electron-hole plasma [56,57]. In the case of MoSe$_2$/WSe$_2$, n_c was measured and theoretically computed to be roughly $n_c \sim 1.6 - 3 \times 10^{-12}$ cm^{-2} [56]. We therefore restrict our analysis to $n < \frac{1}{2}$ and employ HCC, as justified by the experiments.

To study competition between the hopping and non-local interaction terms, we treat moiré excitons as ideal bosons and employ cluster mean-field (CMF) theory [30–34]. As we are using sufficiently small exciton densities, excitons follow to a good approximation bosonic commutation relations, and therefore our bosonic model is well justified [45]. CMF theory has been used in earlier works to investigate nonlocally interacting hard-core bosons in square and triangular lattices, revealing that such systems can feature Mott states, superfluid states, and supersolid phases [31–33]. Moreover, CMF theory has been shown to agree well with Monte Carlo calculations [31,58]. Previous studies have considered only real-valued hopping parameters, whereas here the moiré potential can render t_{NN} complex valued in case of H_H. One therefore cannot apply directly the results of previous studies [31] here.

In the CMF method, a cluster of sufficiently many-lattice sites is solved exactly, and the coupling between the cluster and sites outside the cluster is treated in the mean-field level. Specifically, the cluster Hamiltonian reads

$$H_C = \sum_{i_c,j_c}(t_{i_c j_c} - \mu\delta_{i_c,j_c})x_{i_c}^\dagger x_{j_c} + \sum_{i_c,j_c} U_{i_c j_c} x_{i_c}^\dagger x_{j_c}^\dagger x_{j_c} x_{i_c}$$
$$+ \sum_{i,j_c}(t_{ij_c}\psi_i^* x_{j_c} + \mathrm{H.c.}) + \sum_{i_c,j} 2U_{i_c j} n_j x_{i_c}^\dagger x_{i_c}. \quad (8)$$

Here i_c (i) refers to the sites within (outside) the cluster and we have introduced the chemical potential μ. The mean fields, namely the superfluid order parameter ψ_i and exciton density n_i, are solved selfconsistently. This is done by solving sufficiently many cluster problems, centered at different lattice sites. If site i belongs to M_i different clusters (as clusters can overlap), an average over these clusters is taken, i.e., $\psi_i = \frac{1}{M_i} \sum_C \langle x_i \rangle$, where C is the cluster index (details are provided in SM [45]). The expectation values $\langle x_{i_c} \rangle$ in cluster C are computed by exactly diagonalizing the cluster Hamiltonian H_C and taking the thermal average, i.e., $\langle x_{i_c} \rangle = \frac{1}{Z_C}\mathrm{Tr}\{e^{-\beta H_C} x_{i_c}\}$, where $\beta = k_B T$ with k_B and T being the Boltzmann constant and temperature, and $Z_C = \mathrm{Tr}\{e^{-\beta H_C}\}$ is the partition function for cluster C. Obtained mean fields ψ_i and n_i are inserted back to the cluster Hamiltonian (8) and the iterative procedure is continued till ψ_i and n_i converge for all i. We use several different initial ansatzes for ψ_i and n_i, and select the result with the lowest free energy $\Omega = -k_B T \ln Z$ where Z is the total partition function of the system.

To exactly diagonalize Eq. (8), we consider the Hilbert subspace spanned by the Fock states which have, at maximum, one particle per each site. Moreover, we do not fix the particle number as the average density is controlled by μ in Eq. (8). This ensures that we can access the superfluid order parameter that breaks the $U(1)$-gauge symmetry.

We present in Figs. 3(a) and 3(b) our CMF results for MoSe$_2$/WSe$_2$ as a function of μ and θ, obtained with 10-site clusters (see SM [45]) by using t_{NN}, U_0, and U_{ij} of H_H. To study possible broken spatial symmetries, we define the staggered density as $\Delta n \equiv \frac{\max n_i - \min n_i}{\max n_i}$. We show both the average superfluid order parameter $\bar{\psi}$ [Fig. 3(a)] and Δn [Fig. 3(b)]. For clarity, $\bar{\psi}$, Δn, and average density $\bar{n}$ are also depicted in Figs. 3(c) and 3(d) as a function of θ for $\mu/U_{\mathrm{NN}} = 0.4$ and $\mu/U_{\mathrm{NN}} = 5.8$, respectively.

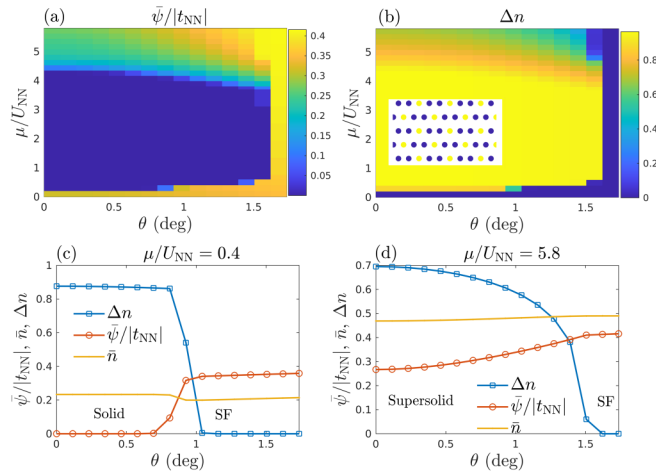FIG. 3. (a) and (b) CMF results for $\bar{\psi}$ and Δn, respectively, as a function of θ and μ at $T = 0$ by using H_H. Inset of panel (b) shows the spatial profile of n_i of the solid phase (yellow denotes $n_i = 1$ and blue $n_i = 0$) with $\bar{n} = 1/3$. (c) and (d) $\bar{\psi}$, Δn, and $\bar{n}$ as a function of θ for $\mu/U_{NN} = 0.4$ and $\mu/U_{NN} = 5.8$, respectively, at $T = 0$.

From Fig. 3 we see that by tuning θ and μ (i.e., $\bar{n}$), one can reach different many-body phases: spatially homogeneous superfluid (SF) phase (characterized by $\bar{\psi} \neq 0$, $\Delta n = 0$), solid phase with broken translational symmetry ($\bar{\psi} = 0$, $\Delta n \neq 0$) and, importantly, supersolid ($\bar{\psi} \neq 0$, $\Delta n \neq 0$). The solid phase has the average density of $\bar{n} = 1/3$ and its spatial density profile, depicted in the inset of Fig. 3(b), is characterized by vanishing density within two-thirds of the sites. The supersolid phase has a similar staggered density pattern, with the exception of having finite density in all the sites so that $\bar{n} > 1/3$.

To study how finite temperature affects the supersolid phase, we plot in Fig. 4(a) $\bar{\psi}$ and Δn as a function of T for $\mu/U_{NN} = 5.88$ at $\theta = 1.4°$ (symbols) and at $\mu/U_{NN} = 5.8$ with $\theta = 0.7°$ (dashed lines). At $\theta = 1.4°$, the superfluid component of the supersolid vanishes around $T \sim 2.4$ K, whereas the staggered density pattern survives to slightly higher temperatures. A similar trend can be seen more clearly in the case of $\theta = 0.7°$ for which the staggered solid phase vanishes at considerably higher temperatures compared to the superfluid order. This is understandable as the superfluidity emerges due to $U(1)$ symmetry breaking and is thus more susceptible
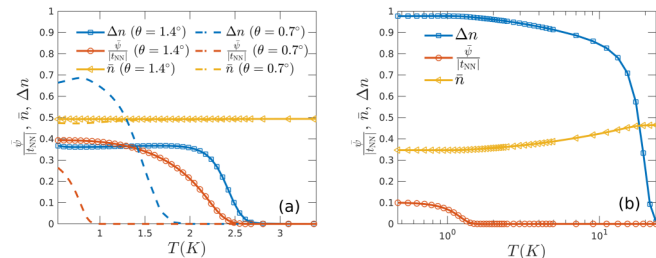
to thermal phase fluctuations. Notably, the superfluid critical temperatures T_c obtained here are experimentally accessible [20,25]. One should note, however, that CMF accounts for exactly local and short-ranged quantum fluctuations, but treats long-range fluctuations in the mean-field level. Thus, CMF most likely overestimates T_c. Our prediction, however, should be better than that given by a simple Gutzwiller mean-field theory. To improve the prediction for T_c, one should perform a fluctuation analysis for the complex phase of ψ_i to access the BKT-transition temperature. With CMF, this could be done as in Ref. [33], where fluctuations of the density matrix were studied, or computing the superfluid density by extending the quantum Gutzwiller theory [59] for our cluster approach. We leave this aspect to future studies.

For completeness, we performed CMF computations for $MoSe_2/WSe_2$ by using t_{NN}, U_0, and U_{ij}, obtained from H_E. With experimentally feasible parameters [16], twist angles of $\theta \sim 3°$ yield supersolidity (see SM [45]). In Fig. 4(b) we show Δn, $\bar{\psi}$, and $\bar{n}$ as a function of T at $\mu/U_{NN} = 5.7$ and $\theta = 3°$. We see that $T_c \sim 1$ K. Our prediction for excitonic supersolidity is thus not model-dependent, but an intrinsic property of moiré excitons that feature a finite interlayer exciton component.

Discussion. We have demonstrated that moiré excitons, in addition to previously predicted Mott and conventional superfluid states [27,28], can also host superfluid and insulating states that break the periodicity of the original triangular moiré lattice. By tuning the density of excitons and the twist angle, one can reach these many-body phases within a reasonable parameter regime and at experimentally accessible temperatures. We employed two different continuum models to build the tight-binding models and interactions for moiré excitons. The common feature of these models is the presence of interlayer excitons. Nontrivial states of broken translational invariance emerge then from strong nonlocal Coulomb interactions, which cannot be ignored in experimentally feasible density regime.

We used here equilibrium CMF theory, whereas experimental systems are inherently in nonequilibrium due to optical pumping and decay processes of excitons. However, interlayer excitons can exhibit relatively long lifetimes in moiré systems; in Ref. [60] the lifetime of interlayer excitons was measured to be around 1–10 nm for small twist angles, giving the decay rate of $\gamma \sim 10^{-4} - 10^{-3}$ meV. This is still much smaller than other energy scales. For example, $|t_{NN}| \sim 0.1$ meV at $\theta \sim 0.7°$ used in Fig. 4(a). Thus, we expect that including a decay term in Eq. (1) does not change our conclusions qualitatively. Moreover, recently realized dual-moiré systems [61,62], where the system geometry suppresses the recombination of electron-hole pairs, can further enhance the lifetime of interlayer excitons and can thus be a strong candidate for realizing supersolid phases similar to the ones predicted here. Nonequilibrium dynamics of excitons provide a rich playground to reveal new properties of moiré systems [60,63] and remain an important topic for future studies.

Our work considers excitons in the K valley only. On the other hand, the hybridized exciton model H_H allows us to simultaneously consider the K'-valley excitons. However, the intralayer excitons of different valleys are coupled via the intervalley exchange interaction [64–66]. Consequently,

FIG. 4. (a) Calculated Δn, $\bar{\psi}$, and $\bar{n}$ as a function of T at $\mu/U_{NN} = 5.88$, $\theta = 1.4°$ (symbols) and at $\mu/U_{NN} = 5.8$, $\theta = 0.7°$ (dashed lines) by using H_H. (b) Corresponding results with H_E for $\mu/U_{NN} = 5.7$ and $\theta = 3°$.

the lowest moiré exciton bands of two valleys hybridize and a two-band tight-binding model is required [67] to faithfully study such intervalley moiré excitons. Intervalley moiré physics can be very rich, e.g., possibly leading to topological band structures [50] and excitonic phases of broken crystal symmetries [68].

Moiré excitons can also easily couple with light, forming moiré exciton polaritons [69] and therefore allowing the creation of strong nonlinearities and many-body phases of light [63,70]. Furthermore, electron-exciton interactions [9,11,12,14,15,25,26,26,71–73] provide a promising platform for studying strongly correlated Bose-Fermi mixtures. Our work, describing the possibility to access supersolid phases, manifests vast opportunities of moiré excitons and highlights their significant role in studying strongly correlated bosonic many-body phases.

[1] L. Balents, C. R. Dean, D. K. Efetov, and A. F. Young, Nat. Phys. **16**, 725 (2020).

[2] D. M. Kennes, M. Claassen, L. Xian, A. Georges, A. J. Millis, J. Hone, C. R. Dean, D. N. Basov, A. N. Pasupathy, and A. Rubio, Nat. Phys. **17**, 155 (2021).

[3] E. Y. Andrei, D. K. Efetov, P. Jarillo-Herrero, A. H. MacDonald, K. F. Mak, T. Senthil, E. Tutuc, A. Yazdani, and A. F. Young, Nat. Rev. Mater. **6**, 201 (2021).

[4] Y. Cao, V. Fatemi, S. Fang, K. Watanabe, T. Taniguchi, E. Kaxiras, and P. Jarillo-Herrero, Nature (London) **556**, 43 (2018).

[5] M. Yankowitz, S. Chen, H. Polshyn, Y. Zhang, K. Watanabe, T. Taniguchi, D. Graf, A. F. Young, and C. R. Dean, Science **363**, 1059 (2019).

[6] G. Chen, A. L. Sharpe, P. Gallagher, I. T. Rosen, E. J. Fox, L. Jiang, B. Lyu, H. Li, K. Watanabe, T. Taniguchi, J. Jung, Z. Shi, D. Goldhaber-Gordon, Y. Zhang, and F. Wang, Nature (London) **572**, 215 (2019).

[7] L. Wang, E.-M. Shih, A. Ghiotto, L. Xian, D. A. Rhodes, C. Tan, M. Claassen, D. M. Kennes, Y. Bai, B. Kim, K. Watanabe, T. Taniguchi, X. Zhu, J. Hone, A. Rubio, A. N. Pasupathy, and C. R. Dean, Nat. Mater. **19**, 861 (2020).

[8] X. Huang, T. Wang, S. Miao, C. Wang, Z. Li, Z. Lian, T. Taniguchi, K. Watanabe, S. Okamoto, D. Xiao, S.-F. Shi, and Y.-T. Cui, Nat. Phys. **17**, 715 (2021).

[9] Y. Shimazaki, I. Schwartz, K. Watanabe, T. Taniguchi, M. Kroner, and A. Imamoğlu, Nature (London) **580**, 472 (2020).

[10] Y. Xu, S. Liu, D. A. Rhodes, K. Watanabe, T. Taniguchi, J. Hone, V. Elser, K. F. Mak, and J. Shan, Nature (London) **587**, 214 (2020).

[11] Y. Tang, L. Li, T. Li, Y. Xu, S. Liu, K. Barmak, K. Watanabe, T. Taniguchi, A. H. MacDonald, J. Shan, and K. F. Mak, Nature (London) **579**, 353 (2020).

[12] A. J. Campbell, M. Brotons-Gisbert, H. Baek, V. Vitale, T. Taniguchi, K. Watanabe, J. Lischner, and B. D. Gerardot, arXiv:2202.08879.

[13] E. Liu, T. Taniguchi, K. Watanabe, N. M. Gabor, Y.-T. Cui, and C. H. Lui, Phys. Rev. Lett. **127**, 037402 (2021).

[14] C. Jin, Z. Tao, T. Li, Y. Xu, Y. Tang, J. Zhu, S. Liu, K. Watanabe, T. Taniguchi, J. C. Hone, L. Fu, J. Shan, and K. F. Mak, Nat. Mater. **20**, 940 (2021).

[15] S. Miao, T. Wang, X. Huang, D. Chen, Z. Lian, C. Wang, M. Blei, T. Taniguchi, K. Watanabe, S. Tongay, Z. Wang, D. Xiao, Y.-T. Cui, and S.-F. Shi, Nat. Commun. **12**, 3608 (2021).

[16] K. Tran, G. Moody, F. Wu, X. Lu, J. Choi, K. Kim, A. Rai, D. A. Sanchez, J. Quan, A. Singh, J. Embley, A. Zepeda, M. Campbell, T. Autry, T. Taniguchi, K. Watanabe, N. Lu, S. K. Banerjee, K. L. Silverman, S. Kim *et al.*, and Nature (London) **567**, 71 (2019).

[17] E. M. Alexeev, D. A. Ruiz-Tijerina, M. Danovich, M. J. Hamer, D. J. Terry, P. K. Nayak, S. Ahn, S. Pak, J. Lee, J. I. Sohn, M. R. Molas, M. Koperski, K. Watanabe, T. Taniguchi, K. S. Novoselov, R. V. Gorbachev, H. S. Shin, V. I. Fal'ko, and A. I. Tartakovskii, Nature (London) **567**, 81 (2019).

[18] D. A. Ruiz-Tijerina and V. I. Fal'ko, Phys. Rev. B **99**, 125424 (2019).

[19] H. Yu, G.-B. Liu, J. Tang, X. Xu, and W. Yao, Sci. Adv. **3**, e1701696 (2017).

[20] K. L. Seyler, P. Rivera, H. Yu, N. P. Wilson, E. L. Ray, D. G. Mandrus, J. Yan, W. Yao, and X. Xu, Nature (London) **567**, 66 (2019).

[21] C. Jin, E. C. Regan, A. Yan, M. Iqbal Bakti Utama, D. Wang, S. Zhao, Y. Qin, S. Yang, Z. Zheng, S. Shi, K. Watanabe, T. Taniguchi, S. Tongay, A. Zettl, and F. Wang, Nature (London) **567**, 76 (2019).

[22] Y. Jiang, S. Chen, W. Zheng, B. Zheng, and A. Pan, Light Sci. Appl. **10**, 72 (2021).

[23] A. R.-P. Montblanch, D. M. Kara, I. Paradisanos, C. M. Purser, M. S. G. Feuer, E. M. Alexeev, L. Stefan, Y. Qin, M. Blei, G. Wang, A. R. Cadore, P. Latawiec, M. Lončar, S. Tongay, A. C. Ferrari, and M. Atatüre, Commun. Phys. **4**, 119 (2021).

[24] D. Huang, J. Choi, C.-K. Shih, and X. Li, Nat. Nanotechnol. **17**, 227 (2022).

[25] X. Wang, C. Xiao, H. Park, J. Zhu, C. Wang, T. Taniguchi, K. Watanabe, J. Yan, D. Xiao, D. R. Gamelin, W. Yao, and X. Xu, Nature (London) **604**, 468 (2022).

[26] E. Liu, E. Barré, J. van Baren, M. Wilson, T. Taniguchi, K. Watanabe, Y.-T. Cui, N. M. Gabor, T. F. Heinz, Y.-C. Chang, and C. H. Lui, Nature (London) **594**, 46 (2021).

[27] N. Götting, F. Lohof, and C. Gies, Phys. Rev. B **105**, 165419 (2022).

[28] C. Lagoin and F. Dubin, Phys. Rev. B **103**, L041406 (2021).

[29] F. Wu, T. Lovorn, and A. H. MacDonald, Phys. Rev. B **97**, 035306 (2018).

[30] D.-S. Lühmann, Phys. Rev. A **87**, 043619 (2013).

[31] D. Yamamoto, I. Danshita, and C. A. R. Sá de Melo, Phys. Rev. A **85**, 021601(R) (2012).

[32] D. Yamamoto, A. Masaki, and I. Danshita, Phys. Rev. B **86**, 054516 (2012).

[33] M. Malakar, S. Ray, S. Sinha, and D. Angom, Phys. Rev. B **102**, 184515 (2020).

[34] S. R. Hassan, L. de Medici, and A.-M. S. Tremblay, Phys. Rev. B **76**, 144420 (2007).

[35] G. Wang, A. Chernikov, M. M. Glazov, T. F. Heinz, X. Marie, T. Amand, and B. Urbaszek, Rev. Mod. Phys. **90**, 021001 (2018).

[36] T. Mueller and E. Malic, npj 2D Mater. Applic. **2**, 29 (2018).

[37] H. Yu, X. Cui, X. Xu, and W. Yao, Natl. Sci. Rev. **2**, 57 (2015).

[38] Y. Wang, Z. Wang, W. Yao, G.-B. Liu, and H. Yu, Phys. Rev. B **95**, 115429 (2017).

[39] D. Xiao, G.-B. Liu, W. Feng, X. Xu, and W. Yao, Phys. Rev. Lett. **108**, 196802 (2012).

[40] T. Cao, G. Wang, W. Han, H. Ye, C. Zhu, J. Shi, Q. Niu, P. Tan, E. Wang, B. Liu, and J. Feng, Nat. Commun. **3**, 887 (2012).

[41] H. Zeng, J. Dai, W. Yao, D. Xiao, and X. Cui, Nat. Nanotechnol. **7**, 490 (2012).

[42] K. F. Mak, K. He, J. Shan, and T. F. Heinz, Nat. Nanotechnol. **7**, 494 (2012).

[43] J. R. Schaibley, H. Yu, G. Clark, P. Rivera, J. S. Ross, K. L. Seyler, W. Yao, and X. Xu, Nat. Rev. Mater. **1**, 16055 (2016).

[44] L. Zhang, R. Gogna, G. W. Burg, J. Horng, E. Paik, Y.-H. Chou, K. Kim, E. Tutuc, and H. Deng, Phys. Rev. B **100**, 041402(R) (2019).

[45] See Supplemental Material at http://link.aps.org/supplemental/10.1103/PhysRevB.106.035406 for details on derivation of H_H and H_E continuum models, details on constructing the tight-binding model, details on computing the interaction terms, derivation of the dielectric functions, details on CMF computations, the results of the weak-coupling Gross-Pitaevskii equation and Bogoliubov theory, and additional Refs. [74–80].

[46] F. Wu, T. Lovorn, E. Tutuc, I. Martin, and A. H. MacDonald, Phys. Rev. Lett. **122**, 086402 (2019).

[47] F. Wu, T. Lovorn, E. Tutuc, and A. H. MacDonald, Phys. Rev. Lett. **121**, 026402 (2018).

[48] H. Pan, F. Wu, and S. Das Sarma, Phys. Rev. Research **2**, 033087 (2020).

[49] N. Morales-Durán, N. C. Hu, P. Potasz, and A. H. MacDonald, Phys. Rev. Lett. **128**, 217202 (2022).

[50] F. Wu, T. Lovorn, and A. H. MacDonald, Phys. Rev. Lett. **118**, 147401 (2017).

[51] M. H. Naik, E. C. Regan, Z. Zhang, Y.-h. Chan, Z. Li, D. Wang, Y. Yoon, C. S. Ong, W. Zhao, S. Zhao, M. I. B. Utama, B. Gao, X. Wei, M. Sayyad, K. Yumigeta, K. Watanabe, T. Taniguchi, S. Tongay, F. H. da Jornada, F. Wang *et al.*, arXiv:2201.02562.

[52] H. Pan, F. Wu, and S. Das Sarma, Phys. Rev. B **102**, 201104(R) (2020).

[53] H. Pan and S. Das Sarma, Phys. Rev. B **105**, L041109 (2022).

[54] H. Pan and S. Das Sarma, Phys. Rev. Lett. **127**, 096802 (2021).

[55] M. Danovich, D. A. Ruiz-Tijerina, R. J. Hunt, M. Szyniszewski, N. D. Drummond, and V. I. Fal'ko, Phys. Rev. B **97**, 195452 (2018).

[56] J. Wang, J. Ardelean, Y. Bai, A. Steinhoff, M. Florian, F. Jahnke, X. Xu, M. Kira, J. Hone, and X.-Y. Zhu, Sci. Adv. **5**, eaax0145 (2019).

[57] J. Wang, Q. Shi, E.-M. Shih, L. Zhou, W. Wu, Y. Bai, D. Rhodes, K. Barmak, J. Hone, C. R. Dean, and X.-Y. Zhu, Phys. Rev. Lett. **126**, 106804 (2021).

[58] S. Wessel and M. Troyer, Phys. Rev. Lett. **95**, 127205 (2005).

[59] F. Caleffi, M. Capone, C. Menotti, I. Carusotto, and A. Recati, Phys. Rev. Research **2**, 033276 (2020).

[60] J. Choi, M. Florian, A. Steinhoff, D. Erben, K. Tran, D. S. Kim, L. Sun, J. Quan, R. Claassen, S. Majumder, J. A. Hollingsworth, T. Taniguchi, K. Watanabe, K. Ueno, A. Singh, G. Moody, F. Jahnke, and X. Li, Phys. Rev. Lett. **126**, 047401 (2021).

[61] Y. Zeng, Z. Xia, R. Dery, K. Watanabe, T. Taniguchi, J. Shan, and K. F. Mak, arXiv:2205.07354.

[62] Y.-H. Zhang, arXiv:2204.10937.

[63] A. Camacho-Guardian and N. R. Cooper, Phys. Rev. Lett. **128**, 207401 (2022).

[64] H. Yu, G.-B. Liu, P. Gong, X. Xu, and W. Yao, Nat. Commun. **5**, 3876 (2014).

[65] T. Yu and M. W. Wu, Phys. Rev. B **89**, 205303 (2014).

[66] F. Wu, F. Qu, and A. H. MacDonald, Phys. Rev. B **91**, 075310 (2015).

[67] N. Marzari and D. Vanderbilt, Phys. Rev. B **56**, 12847 (1997).

[68] B. Remez and N. R. Cooper, Phys. Rev. Research **4**, L022042 (2022).

[69] L. Zhang, F. Wu, S. Hou, Z. Zhang, Y.-H. Chou, K. Watanabe, T. Taniguchi, S. R. Forrest, and H. Deng, Nature (London) **591**, 61 (2021).

[70] A. Camacho-Guardian and N. R. Cooper, arXiv:2206.06166.

[71] E. Marcellina, X. Liu, Z. Hu, A. Fieramosca, Y. Huang, W. Du, S. Liu, J. Zhao, K. Watanabe, T. Taniguchi, and Q. Xiong, Nano Lett. **21**, 4461 (2021).

[72] Y. Tang, J. Gu, S. Liu, K. Watanabe, T. Taniguchi, J. Hone, K. F. Mak, and J. Shan, Nat. Nanotechnol. **16**, 52 (2021).

[73] X. Wang, J. Zhu, K. L. Seyler, P. Rivera, H. Zheng, Y. Wang, M. He, T. Taniguchi, K. Watanabe, J. Yan, D. G. Mandrus, D. R. Gamelin, W. Yao, and X. Xu, Nat. Nanotechnol. **16**, 1208 (2021).

[74] H. Yu, Y. Wang, Q. Tong, X. Xu, and W. Yao, Phys. Rev. Lett. **115**, 187002 (2015).

[75] P. Rivera, K. L. Seyler, H. Yu, J. R. Schaibley, J. Yan, D. G. Mandrus, W. Yao, and X. Xu, Science **351**, 688 (2016).

[76] D. Leykam, A. Andreanov, and S. Flach, Adv. Phys.: X **3**, 1473052 (2018).

[77] R. Bistritzer and A. H. MacDonald, Proc. Natl. Acad. Sci. USA **108**, 12233 (2011).

[78] M. Angeli and A. H. MacDonald, Proc. Natl. Acad. Sci. USA **118**, e2021826118 (2021).

[79] Y. Castin, in *Coherent Atomic Matter Waves*, edited by R. Caiser, C. Westbrook, and F. David (EDP Sciences and Springer-Verlag, 2001).

[80] S. A. Moskalenko and D. W. Snoke, *Bose-Einstein Condensation of Excitons and Biexcitons and Coherent Nonlinear Optics with Excitons* (Cambridge University Press, 2000).